








IFN signaling and neutrophil degranulation transcriptional signatures are induced during SARS-CoV-2 infection

Bruce A. Rosa ^{1,6}, Mushtaq Ahmed^{2,6}, Dhiraj K. Singh ^{3,6}, José Alberto Choreño-Parra⁴, Journey Cole³, Luis Armando Jiménez-Álvarez⁴, Tatiana Sofía Rodríguez-Reyna ⁵, Bindu Singh³, Olga Gonzalez³, Ricardo Carrion Jr. ³, Larry S. Schlesinger³, John Martin¹, Joaquín Zúñiga ⁴, Makedonka Mitreva ¹✉, Deepak Kaushal ³✉ & Shabaana A. Khader²✉

SARS-CoV-2 virus has infected more than 92 million people worldwide resulting in the Coronavirus disease 2019 (COVID-19). Using a rhesus macaque model of SARS-CoV-2 infection, we have characterized the transcriptional signatures induced in the lungs of juvenile and old macaques following infection. Genes associated with Interferon (IFN) signaling, neutrophil degranulation and innate immune pathways are significantly induced in macaque infected lungs, while pathways associated with collagen formation are downregulated, as also seen in lungs of macaques with tuberculosis. In COVID-19, increasing age is a significant risk factor for poor prognosis and increased mortality. Type I IFN and Notch signaling pathways are significantly upregulated in lungs of juvenile infected macaques when compared with old infected macaques. These results are corroborated with increased peripheral neutrophil counts and neutrophil lymphocyte ratio in older individuals with COVID-19 disease. Together, our transcriptomic studies have delineated disease pathways that improve our understanding of the immunopathogenesis of COVID-19.

¹Department of Medicine, Washington University in St. Louis, St. Louis, MO, USA. ²Department of Molecular Microbiology, Washington University in St. Louis, St. Louis, MO, USA. ³Southwest National Primate Research Center, Texas Biomedical Research Institute, San Antonio, TX, USA. ⁴Laboratory of Immunobiology and Genetics, Instituto Nacional de Enfermedades Respiratorias Ismael Cosío Villegas, Mexico City, Mexico. ⁵Department of Immunology and Rheumatology, Instituto Nacional de Ciencias Médicas y Nutrición Salvador Zubirán, Mexico City, Mexico. ⁶These authors contributed equally: Bruce A. Rosa, Mushtaq Ahmed, Dhiraj K. Singh. ✉email: mmitreva@wustl.edu; dkaushal@txbiomed.org; sakhader@wustl.edu

Coronavirus disease 2019 (COVID-19), caused by the novel severe acute respiratory syndrome coronavirus 2 (SARS-CoV-2), emerged as a pandemic disease during the end of 2019 and the beginning of 2020. Infected individuals develop a cytokine storm¹, which can initiate viral sepsis and inflammation-induced lung injury leading to complications including pneumonia, acute respiratory distress syndrome (ARDS), respiratory failure, shock, organ failure, and potentially death^{1,2}.

By combining established principles of anti-viral immunity with analysis of immune responses in COVID-19 patients, a picture of the host defense response against SARS-CoV-2 is beginning to emerge^{3,4}. Upon infection of the mucosal epithelium, SARS-CoV-2 is detected by intracellular pattern recognition receptors (PRRs) that bind viral RNA and DNA. PRR signaling triggers activation of transcription factors and induces Interferon (IFN) signaling, which in turn activates resident macrophages. Infected macrophages induce cytokine secretion that consequently triggers the recruitment of myeloid cells, likely resulting in a feed-back loop that aggravates immunopathogenesis and promotes disease progression.

Analyses of the transcriptomic response of host cells upon virus infection have the potential to identify the host immune response dynamics and gene activated regulatory networks^{5,6}. Recent studies have reported transcriptional changes in cells in the broncho-alveolar lavage (BAL) and peripheral blood mononuclear cells (PBMCs) of COVID-19 patients^{7–11}. Single-cell RNA-seq has recently identified initial cellular targets of SARS-CoV-2 infection in model organisms¹² and patients¹³ characterizing peripheral and local immune responses in severe COVID-19¹⁴, thereby associating the severe disease with a cytokine storm and increased neutrophil accumulation. However, most studies have been performed in a limited number of moderate or severe COVID-19 patients within limited age ranges¹⁴. To get more in-depth understanding of the transcriptional changes during COVID-19, we have developed a SARS-CoV-2 macaque model, where both juvenile and old macaques were infected and exhibited clinical symptoms that reflect human COVID-19 disease that is self-limiting. In the current study, we have characterized the transcriptional signatures induced in the lungs of juvenile and old rhesus macaques following SARS-CoV-2 infection. We show that genes associated with IFN signaling, neutrophil degranulation, and innate immune pathways are significantly induced in the lungs in response to SARS-CoV-2 infection. This is associated with a downregulation of genes associated with collagen formation and regulation of collagen pathways. In COVID-19, increasing age is a significant risk factor for poor prognosis of infection¹⁵. We demonstrate that specific immune pathways, namely Type I IFN and Notch signaling, are significantly

upregulated in juvenile macaques when compared with old macaques infected with SARS-CoV-2. These results are corroborated with increased peripheral neutrophil counts and neutrophil-lymphocyte ratio in older individuals with COVID-19 disease. In contrast, the VEGF pathway is downregulated in old infected macaques. Incidentally, levels of VEGF protein are increased in plasma of older COVID-19 patients, emphasizing the importance of studying both local and peripheral responses. Finally, we report that neutrophil degranulation, innate immune system, and IFN gamma (IFN- γ) signaling pathways are upregulated in both tuberculosis (TB) and COVID-19, two pulmonary infectious diseases where neutrophils accumulation is associated with increased severity. Together, our study has delineated disease pathways that can serve as a valuable tool in understanding the immunopathogenesis of SARS-CoV-2 infection and progressive COVID-19.

Results

Genes upregulated in COVID-19 infected macaques represent pathways characteristic of neutrophil degranulation and IFN signaling. We recently assessed the ability of SARS-CoV-2 to infect rhesus macaques during a longitudinal two-week infection study¹⁶. Indian-origin, SPF-rhesus macaques (*Macaca mulatta*) were infected by multiple routes (ocular, intratracheal, and intranasal) with the sixth-passage virus at a target dose of 1.05×10^6 PFU/per animal and studied for two weeks. The macaques were grouped as naïve (uninfected), and infected (juvenile or old) macaques. All infected animals developed clinical signs of viral infection¹⁶. Both juvenile and old macaques exhibited comparable clinical disease, and equivalent longitudinal viral loads in the BAL, nasopharyngeal and buccopharyngeal swabs, as well as lungs at endpoint. This was followed by comparable viral clearance. In the current study in order to fully understand the immune pathways regulated upon SARS-CoV-2 infection, RNA was extracted and RNA sequencing was carried out from a lung biopsy from juvenile macaques ($n = 3$, 1 male and 2 females) and old macaques infected with SARS-CoV-2 ($n = 5$, 1 male and 4 females) and naïve uninfected macaques ($n = 4$, 2 males and 2 females) (Supplementary Data 1). An average of 68.6 million reads was generated, with an average of 20.3 million fragments (read pairs or orphaned reads) mapping to macaque coding sequences, following analytical processing and mapping (Supplementary Data 1). Principal components analysis (PCA) based on whole-transcriptome gene expression levels¹⁷ showed that despite within-group variability for the COVID-19 infected samples, the naïve samples grouped separately, suggesting substantial overall transcriptomic differences resulting from the infection (Fig. 1a). Differential gene expression analysis

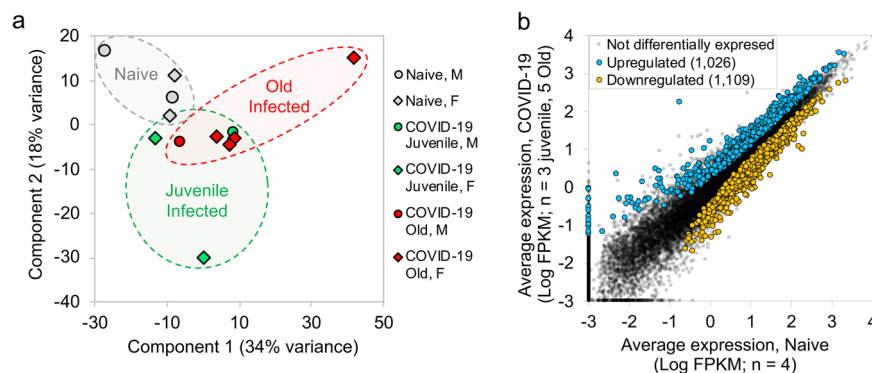


Fig. 1 Gene expression profiles for lung tissue samples from macaques infected with SARS-CoV-2 are distinct from naïve uninfected samples. **a** PCA plot showing the clustering of samples based on overall transcriptomic profiles. **b** Differential gene expression plot showing the relative normalized gene expression levels (FPKM) for each gene, with genes significantly differentially regulated by COVID-19 are indicated.

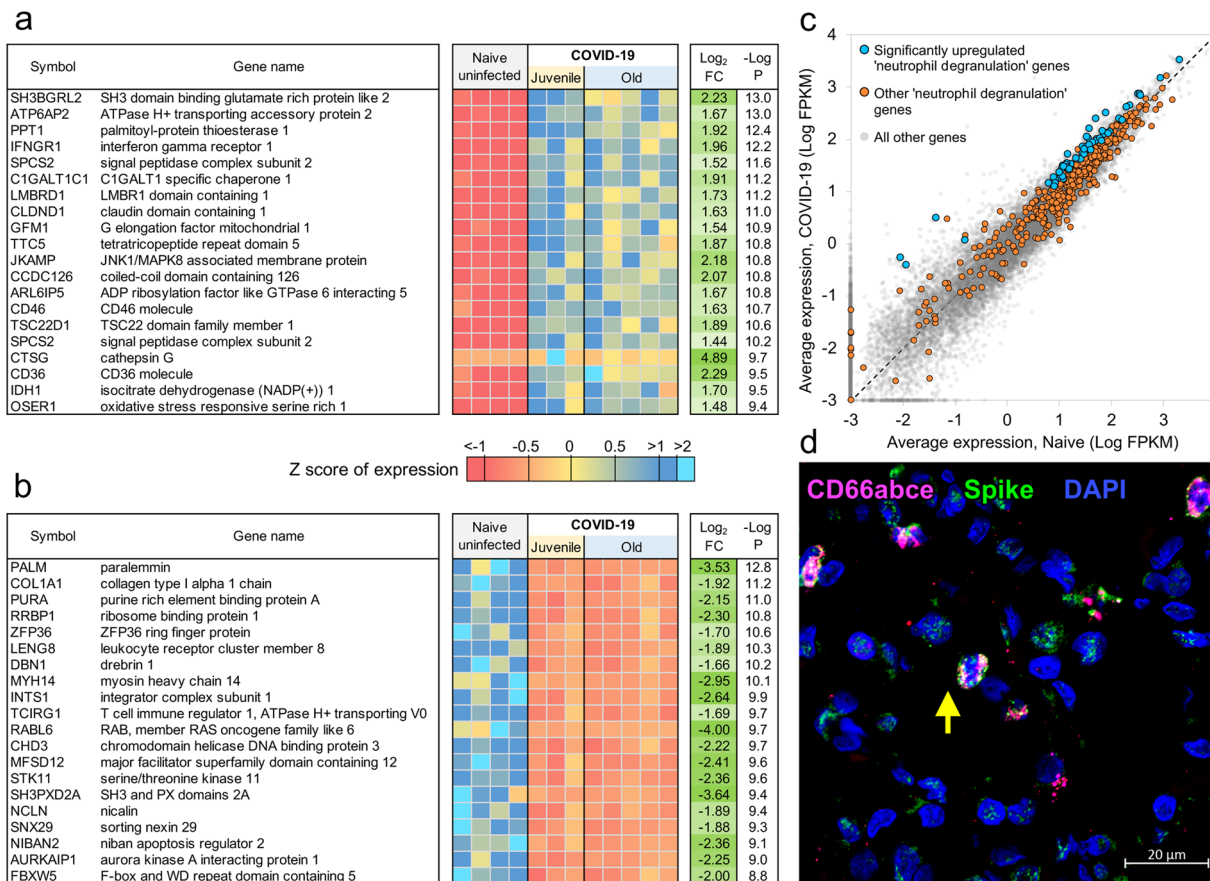


Fig. 2 Genes differentially regulated in SARS-CoV-2-infected macaques represent pathway characteristic of neutrophil degranulation, IFN signaling, collagen degradation and TFG-β signaling. The top 20 most significantly **a** upregulated genes and **b** downregulated genes in SARS-CoV-2-infected macaque lungs. Expression values are visualized by Z scores of normalized expression data (FPKM) per sample, and Log₂ Fold Change and -Log P values are from the DESeq2 output. Genes are sorted by P value. **c** Gene expression plot showing the relative normalized gene expression levels (FPKM) for each gene, with “neutrophil degranulation” (R-HSA-6798695) pathway genes highlighted, including those that were significantly upregulated during COVID-19 (blue) and those that were not (orange). **d** Multilabel confocal immunofluorescence microscopy of FFPE lung sections from SARS-CoV-2-infected rhesus macaques with SARS-CoV-2 Spike specific antibody (green), neutrophil marker CD66abce (red), and DAPI (blue) at 63X magnification.

(DESeq2¹⁷) with the juvenile and old COVID-19 samples grouped together identified 1,026 genes significantly ($P \leq 0.01$) upregulated in response to infection, while 1109 genes were significantly downregulated (Fig. 1b). Expression, annotation, and differential expression data for all genes is available in Supplementary Data 2. Complete lists of differentially expressed genes for each comparison of interest (described below) ranked by P value, with Z-scores for expression visualization are available in Supplementary Data 3, and significant pathway enrichment (Reactome¹⁸, KEGG¹⁹, and Gene Ontology²⁰) for all comparisons is shown in Supplementary Data 4.

Evaluation of the top 30 most significantly upregulated genes in the lungs of SARS-CoV-2-infected macaques revealed significantly higher expression of *CTSG* (Cathepsin G), *ATP6AP2* (ATPase H+ transporting accessory protein 2), *IFNγR1* (Interferon Gamma Receptor), *CD36*, and *CD58*, in comparison to expression in uninfected macaque lungs (Fig. 2a). Cathepsin G is a serine protease prominently found in neutrophilic granules. *IFNγR1* associates with *IFNγR2* to form a receptor for the cytokine interferon gamma (*IFNγ*)^{21–24}, and required for activation of antiviral responses, such as *IRF3* (IFN regulatory factor-3), nuclear factor KB (NF-KB) and *JAK* (Janus kinase)/*STAT* (signal transducer and activator of transcription) signaling pathways²⁵. Reactome pathway analysis on upregulated and downregulated genes in the lungs of SARS-CoV-2-infected rhesus

macaques showed that genes significantly upregulated by infection, included pathway enrichment for genes involved in “Neutrophil degranulation”, “Innate Immune system”, “Immune system” and “IFN signaling” (Supplementary Table 1 and Supplementary Data 4A). The upregulation of *CD36* during COVID-19 in lungs is in conformity with these enriched pathways, since *CD36*, a scavenger receptor expressed in multiple cell types, mediates lipid uptake, immunological recognition, inflammation, molecular adhesion, and apoptosis²⁶, and is a Matrix Metalloproteinase-9 substrate that induces neutrophil apoptosis. *CD58* molecule (lymphocyte function-associated antigen-3) is expressed on human hematopoietic and non-hematopoietic cells, including dendritic cells, macrophages, and endothelial cells^{27–30}, and interacts with its receptor *CD2* molecule^{31,32} on *CD8+* cytotoxic T lymphocytes and NK cells to mediate cytotoxic reactions^{33–35}. The complete ranked list of the 1026 genes upregulated during COVID-19 is shown in Supplementary Data 3A.

ATP6AP2 was the most significant of the 65 genes upregulated within the enriched “neutrophil degranulation” (R-HSA-6798695) pathway (Supplementary Data 3B). It interacts with renin or prorenin to cause activation of intracellular signaling pathways, resulting in secretion of inflammatory and fibrotic factors³⁶. *CEACAM8* (Carcinoembryonic Antigen-Related Cell Adhesion Molecule 8) is the gene that encodes for *CD66b*,

a well-characterized marker of degranulation³⁷. Significant upregulation of neutrophil degranulation genes was observed in SARS-CoV-2-infected macaques (Fig. 2c). Indeed, CD66b⁺ neutrophils accumulate in the lungs of macaques infected with SARS-CoV-2 (Fig. 2d). We have also previously demonstrated that neutrophils are heavily recruited early to the alveolar space following SARS-CoV-2 infection of macaques¹⁶. Additional genes strongly upregulated during COVID-19 in the neutrophil degranulation pathway are *IDH-1* (Isocitrate Dehydrogenase (NADP(+)) 1) which regulates neutrophil chemotaxis, and *FPR2* (Formyl Peptide Receptor 2), a G-coupled surface receptor which has a deleterious role to play in viral infection including influenza³⁸. LTA4H (Leukotriene A4 hydrolase) is an enzyme that generates a neutrophil chemoattractant, leukotriene B4, a marker for ARDS³⁹. Expression of 162 genes belonging to the “immune system” (R-HSA-168256) pathway was upregulated in SARS-CoV-2 infected macaques (Supplementary Data 3C). These included *LAMP-2* (Lysosomal Associated Membrane Protein 2), and *ATG7* (Autophagy Related 7), key genes involved in autophagy. *LAMP-2* is known to influence phagosomal maturation in neutrophil⁴⁰. The IFN response constitutes the major first line of defense against viruses. Consistent with this, we found upregulation of genes associated with the IFN signaling pathways, specifically Interferon Induced Protein with Tetratricopeptide Repeats 1 (*IFIT3*), IFN alpha receptor 1 (*IFNAR1*), IFN gamma receptor 1 (*IFNGR1*), and OAS 1 protein (2'-5'-*Oligoadenylate Synthetase 1*). Together, these results suggest that upregulation of neutrophil degranulation, Type I IFN signaling, and the innate immune system is a characteristic feature of host responses to SARS-CoV-2 infection.

Genes downregulated following SARS-CoV-2 infection in macaques represent pathways characteristic of collagen degradation and TGF- β signaling. Up to 40% of patients with COVID-19 develop ARDS, and 20% of ARDS cases are severe⁴¹. A well-documented sequela of ARDS is the development of fibrotic disease^{42,43}. We found that the 1109 genes downregulated in SARS-CoV-2-infected macaques were significantly enriched for collagen degradation, regulation, and formation (Fig. 2b, Supplementary Table 2; Supplementary Data 3D and Supplementary Data 4B). For example, among the “collagen degradation” (R-HSA-1442490) enriched pathway genes (Supplementary Data 3E), *COL1A1* (collagen type I chain), other members of the collagen gene family (*COL4A2 COL16A1 COL4A4 COL6A2 COL6A1 COL5A1 COL9A1 COL13A1 COL12A1 COL1A2*) were all significantly downregulated in COVID-19 diseased lungs when compared with expression in lungs of uninfected controls. Although matrix metalloproteinase (MMPs) are proteolytic enzymes responsible for extracellular matrix protein degradation, in our study matrix metalloproteinases such as MMP23B, MMP15 and MMP14 were downregulated in COVID-19 diseased lungs compared with expression in lungs of uninfected controls. In addition, Reactome pathway enrichment prominently featured pathways downregulated in COVID-19 disease in macaques comprised of “collagen degradation”, “collagen chain trimerization”, “degradation of extracellular matrix” and “collagen formation” (Supplementary Table 2). Increased collagen degradation is essential for the prevention of fibrosis, a sequela of COVID-19 and ARDS. Therefore, regulation of collagen degradation and extracellular matrix modeling suggests that this may be a feature of SARS-CoV-2 infection of rhesus macaques being a self-limiting model with early and robust anamnestic responses. TGF β (Transforming Growth Factor Beta 1) is involved in normal tissue repair following lung injury, and in mediating fibrotic tissue remodeling by increasing the production and decreasing the

degradation of connective tissue⁴⁴. Our results indicate downregulation of genes associated with TGF β signaling (Supplementary Table 2), including the genes *PARD3* (par-3 family cell polarity regulator) and *PARD6A* (par-6 family cell polarity regulator alpha), which are involved in regulating epithelial cell apico-basolateral polarization, *SMURF* (SMAD specific E3 ubiquitin-protein ligase 1), a negative regulator of TGF β pathway, and *FURIN*, which is a TGF β converting enzyme (Supplementary Data 3F). While the interaction of the genes within these pathways is complex, our results project a broad downregulation of mechanisms that contribute to lung repair and remodeling in animals with anamnestic control of SARS-CoV-2 infection.

Type I IFN signaling and Notch signaling pathways are upregulated in young macaques but not old macaques with COVID-19 disease. Age is a significant risk factor for increased morbidity and mortality in COVID-19 disease¹⁵. In order to identify the differential immune responses associated with SARS-CoV-2 infection in old macaques, we carried out differential expression analysis between juvenile ($n = 3$) vs naive ($n = 4$), and old ($n = 5$) vs naive ($n = 4$) groups. In order for a gene to be considered to be differentially expressed only in the juvenile macaques, we required a stringent P value for significance ≤ 0.01 in the juvenile COVID-19 vs naive, and a P value for significance ≥ 0.1 in the old COVID-19 vs naive comparison. This approach identified 86 genes significantly upregulated (Fig. 3a and Supplementary Data 3G) and 96 genes significantly downregulated (Fig. 3b and Supplementary Data 3H) with COVID-19 disease only in juveniles. Note that no genes were significantly upregulated in juveniles and significantly downregulated in old, and vice-versa. Of these genes, the top 30 most significantly differential between juvenile and old are shown for upregulated genes in Fig. 4a and for downregulated genes in Fig. 4b. No pathways were found to be significantly enriched among the 96 genes significantly downregulated only in juveniles, but the Reactome and KEGG pathways significantly enriched among the 86 genes upregulated only in juveniles are shown in Supplementary Table 3. Complete gene lists per pathway, and all significant pathways enrichment results including for Gene Ontology (GO) are available in Supplementary Data 4C.

The genes with significantly upregulated expression in SARS-CoV-2 infected juvenile but not old macaques included *MX1* (MX Dynamin Like GTPase 1), *MX2* (MX Dynamin Like GTPase 2), and *USP18* (Ubiquitin Specific Peptidase 18) (Fig. 5a, b). This is consistent with and highlights the role of the Reactome pathway “interferon alpha/beta signaling” being enriched in juvenile macaques during SARS-CoV-2 infection (Supplementary Table 3 and Supplementary Data 4C). Other genes in this pathway that exhibited increased expression included *IFIT1* and *IFIT2* (Fig. 5a, b). In addition, by KEGG analysis, the Notch signaling pathway was observed to be significantly upregulated in juvenile infected macaques when compared with old infected macaques. *ADAM17* (ADAM Metalloproteinase Domain 17), a key component of the Notch signaling pathways is known to be involved in the shedding of the surface protein ACE2 (Angiotensin-converting enzyme 2)⁴⁵. Therefore, it is interesting that a linear correlation in the expression of ACE2 and *ADAM17* exists in infected macaques (Fig. 4c). Note that we also see a significant upregulation of *ACE2* across SARS-CoV-2-infected samples and a substantially larger upregulation among the juvenile samples (7.1-fold, $P = 3.4 \times 10^{-4}$). In addition, the induction of *DLL4*, a Notch ligand, was increased in the infected juvenile macaques. Finally, the differential induction of *DTX3L* (Deltex E3 Ubiquitin Ligase 3L) in juvenile infected macaques compared to old infected macaques is important because Deltex stabilizes the receptor in

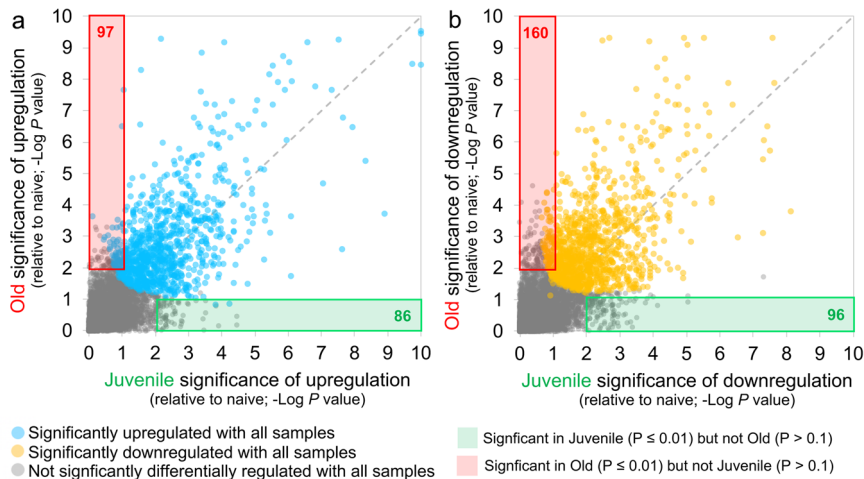


Fig. 3 86 genes were significantly upregulated and 96 genes were significantly downregulated with COVID-19 only in juvenile macaques. Heatmaps visualizing the significance values of COVID-19 a upregulated and b downregulated genes, in juvenile and old macaques. Green shaded areas contain genes significant only in juveniles, and red shaded areas contain genes significant only in old macaques.

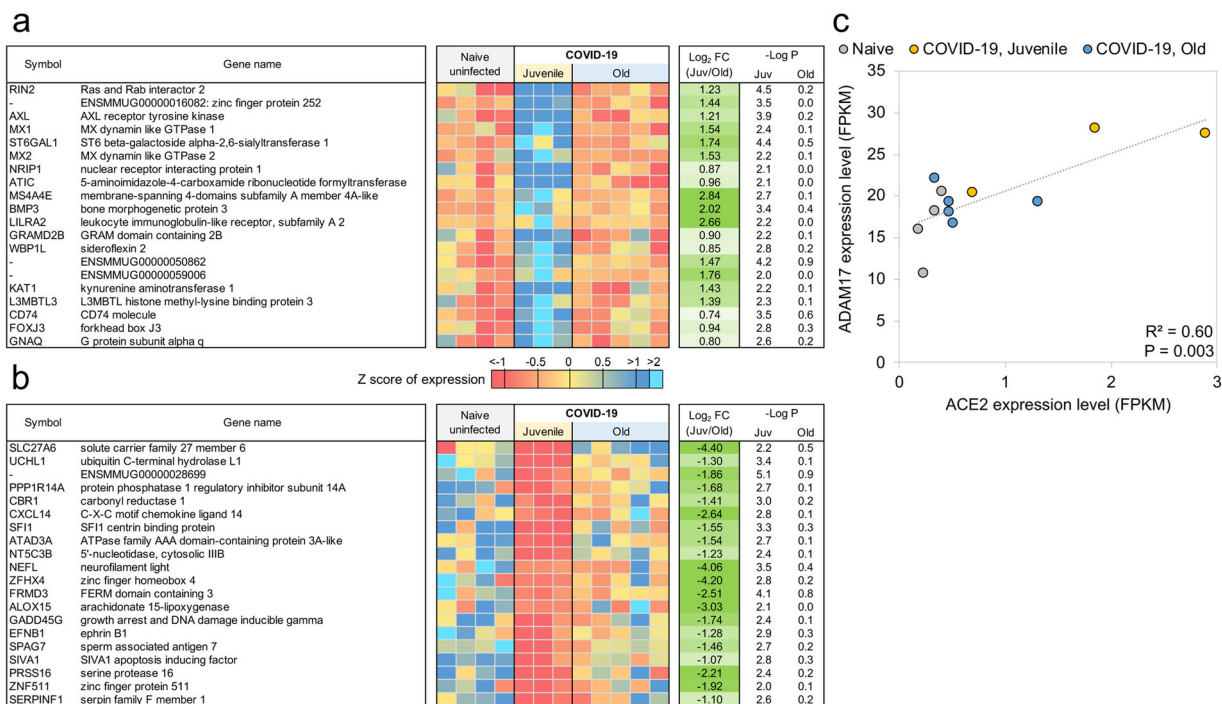


Fig. 4 Genes related to Type I interferon signaling are upregulated in juvenile macaques compared to old macaques during COVID-19-infection. The top 20 most significantly a upregulated genes and b downregulated genes in SARS-CoV-2 infected juvenile macaque lungs but not in old macaques. Expression values are visualized by Z scores of normalized expression data (FPKM) per sample, and Log₂ Fold Change and -Log P values are from the DESeq2 output. Genes are sorted by P value. c The relative gene expression of ACE2 and ADAM17 among naive, juvenile and old SARS-CoV-2-infected macaques.

the endocytic compartment allowing signal transduction to proceed in Notch signaling⁴⁶. Of the Hepatitis-induced pathway genes that are upregulated in juvenile COVID-19 diseased lungs, CXCL-10 (C-X-C Motif Chemokine Ligand 10) is a chemokine associated with severe disease in COVID-19 in humans⁴⁷, but can also be involved in the recruitment of CXCR3 (C-X-C Motif Chemokine Receptor 3) expressing immune cells. 14-3-3 (otherwise called YWHAG) interacts with MDA5 (melanoma differentiation-associated protein 5), which belongs to the RIG-I-like receptor family and drive anti-viral immunity. Together, these results suggest that specific pathways including Type I IFN and Notch signaling are highly induced in juvenile macaques

during SARS-CoV-2 infection, when compared to similarly infected old macaques.

Genes related to VEGF signaling are downregulated in old macaques but not juvenile macaques during COVID-19-disease. Using the same approach as for the juvenile macaque-specific differentially regulated genes, we identified 97 genes significantly upregulated (Fig. 3a and Supplementary Data 3I) and 160 genes significantly downregulated (Fig. 3b and Supplementary Data 3J) with COVID-19 disease only in infected old macaques, and not infected juveniles. Pathway enrichment

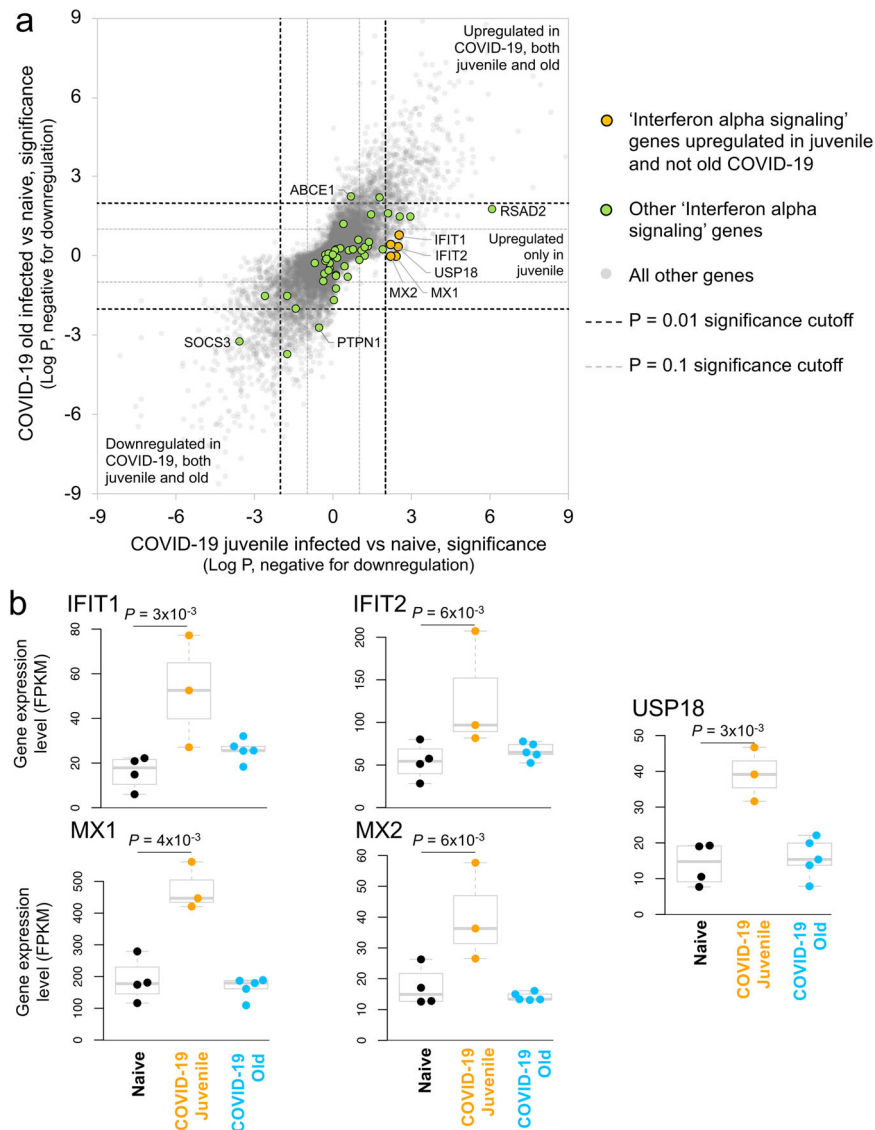


Fig. 5 Interferon alpha signaling genes are significantly upregulated in juvenile SARS-CoV-2-infected macaques but not old SARS-CoV-2-infected macaques. **a** Differential expression significance values for genes from the “Interferon-alpha signaling” (R-HSA-909733) pathway, in both the juvenile vs naive and old vs naive comparisons. Included are significance values for all genes (gray), pathway genes significantly upregulated in juvenile but not old (orange) and other pathway genes (green). P value cutoffs (0.01 and 0.1) are indicated with dashed lines. **b** The relative expression levels (FPKM) for the five “interferon-alpha signaling” genes belonging to this gene set are shown. P values represent FDR-corrected significance values from DESeq2.

analysis only identified significant functional enrichment among the downregulated gene set (Supplementary Table 4 and Supplementary Data 4D). Our results show that in the lungs of old macaques, the only Reactome pathways enriched among genes downregulated during COVID-19 included genes involved in the “VEGF-VEGFR2 Pathway” and “Signaling by VEGF” (Figs. 6a, b and 7a, b). Vascular endothelial growth factor (VEGF) is a signaling protein that promotes angiogenesis, and is a key factor that promotes ARDS. Previous research depicts that ACE2 antagonizes and down-regulates VEGFA⁴⁸, improving lung function following acute lung injury⁴⁹. Here, we observe both a significant increase in *ACE2* in response to COVID-19 and a significant decrease in *VEGF* pathways in old macaques, which may be due to this antagonistic relationship. VEGFA, p21-activated kinase (PAK2), cytoplasmic tyrosine kinase (SRC), RhoA/ROCK signaling [ROCK1(Rho Associated Coiled-Coil Containing Protein Kinase 1) and WASF2 (WASP Family Member 2) are all essential for multiple aspects of VEGF-mediated angiogenesis and are all

significantly downregulated in old macaques with COVID-19 (Fig. 7a, b). Overall, despite juvenile and old macaques having a comparable clinical course with resolution, our data suggest that there are significant differences in signaling pathways, especially those related to VEGF signaling that may ultimately result in differences in long-term outcomes. Thus, our results suggest that downregulation of VEGF pathways is associated with increasing age, in a macaque model of the self-limiting disease.

Aged COVID-19 patients exhibit increased plasma VEGF protein levels and high peripheral neutrophil to lymphocyte ratio. To further address if our findings were relevant in the human setting of SARS-CoV-2 infection, we stratified COVID-19 patients into an aged group (>60 years) and a group of COVID-19 patients <60 years (Supplementary Data 5). We found that with increasing age, there was an increased association of disease parameters and comorbidities (Supplementary Data 5). We measured the levels of human plasma proteins levels for IFN- α ,

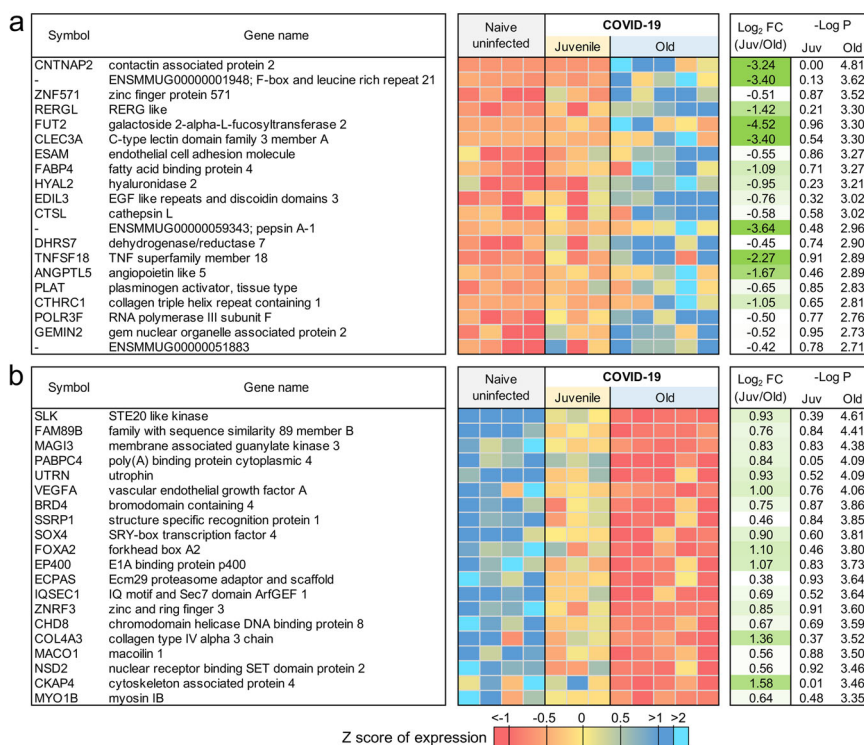


Fig. 6 Genes related to VEGF signaling are downregulated in old macaques compared to juvenile macaques during COVID-19. The top 20 most significantly **a** upregulated genes and **b** downregulated genes in infected old macaque lungs but not in juvenile macaques. Expression values are visualized by Z scores of normalized expression data (FPKM) per sample, and Log₂ fold change and -Log P values are from the DESeq2 output. Genes are sorted by P value.

IFN-β, and IFN-γ. While levels of plasma IFN-α, and IFN-β were below the levels of reliable detection, we found that the COVID-19 patients who were <60 years expressed significantly higher plasma IFN-γ levels when compared to levels in the plasma of healthy controls (Fig. 8a). Although plasma levels of IFN-γ protein were also increased in the aged COVID-19 patient group, levels were not significantly different from healthy controls (Fig. 8a). This was in contrast to plasma protein levels of VEGF, which were significantly higher in aged individuals with COVID-19 disease when compared with levels in individuals with COVID-19 disease who were <60 years old (Fig. 8b). The increased levels of VEGF in aged COVID-19 patients coincided with significantly increased peripheral neutrophil counts as well as increased peripheral neutrophil to lymphocyte ratios, when compared with both healthy controls and COVID-19 group <60 years old (Fig. 8c, d). These results show that plasma protein levels of VEGF and accumulation of peripheral neutrophils is increased in aged individuals with COVID-19 disease, when compared to younger individuals with COVID-19 disease.

Neutrophil degranulation and IFN pathways overlap between COVID-19 and TB disease. TB is a pulmonary granulomatous disease caused by infection with *Mycobacterium tuberculosis*. TB disease in humans and macaques is associated with neutrophil and IFN signature⁵⁰. Thus, we next compared and contrasted the transcriptional profile of genes and pathways that are shared by the two diseases, and those that are unique to COVID-19. There was not a substantial overlap between differentially expressed genes in response to COVID-19 and TB. However, of the 97 genes that were commonly upregulated in TB and COVID-19 (Fig. 9a and Supplementary Data 3K), the Reactome pathway enrichment was well featured in “Neutrophil degranulation”, “Innate immune response”, and “Interferon-gamma signaling”

(Fig. 9b and Supplementary Data 4E). Nearly as many genes (76) had opposite differential expression patterns (upregulated in COVID-19, downregulated in TB), as genes upregulated in both diseases (Fig. 10a and Supplementary Data 3L). These genes were associated with blood vessel morphogenesis and angiogenesis including leptin receptor (*LEPR*) and TGFβ2 (Fig. 10b and, Supplementary Data 4F). These results suggest that both TB and COVID-19 share features of neutrophil accumulation of IFN signaling, but that COVID-19 disease immunopathogenesis uniquely features vascularization of the lung.

Discussion

Lack of understanding of the complexity of COVID-19 immunopathogenesis hampers the identification of therapeutic strategies for COVID-19. While immune profiling in COVID-19 patients has shed light on related immune mechanisms of this disease, this approach has primarily involved peripheral samples obtained from moderate to severe COVID-19 patients, who are generally also older. To overcome these limitations and serve as a hypothesis-generating platform, we have developed a nonhuman primate model (rhesus macaque) of SARS-CoV-2 infection. This model reflects several features of the immunopathogenesis of human COVID-19, and allows us to interrogate the immune pathways that mediate disease versus protection, especially in the context of young versus older hosts. In this study, we show that upregulation of pathways characteristic of neutrophil degranulation and IFN signaling are characteristic of COVID-19 disease in infected hosts. Importantly, the induction of genes associated with Type I IFN signaling pathway and Notch signaling in young macaques infected with SARS-CoV-2 is a key determinant that distinguishes them from infected old macaques. Lungs of old macaques infected with COVID-19 however, uniquely feature downregulation of VEGF signaling pathways. Importantly,

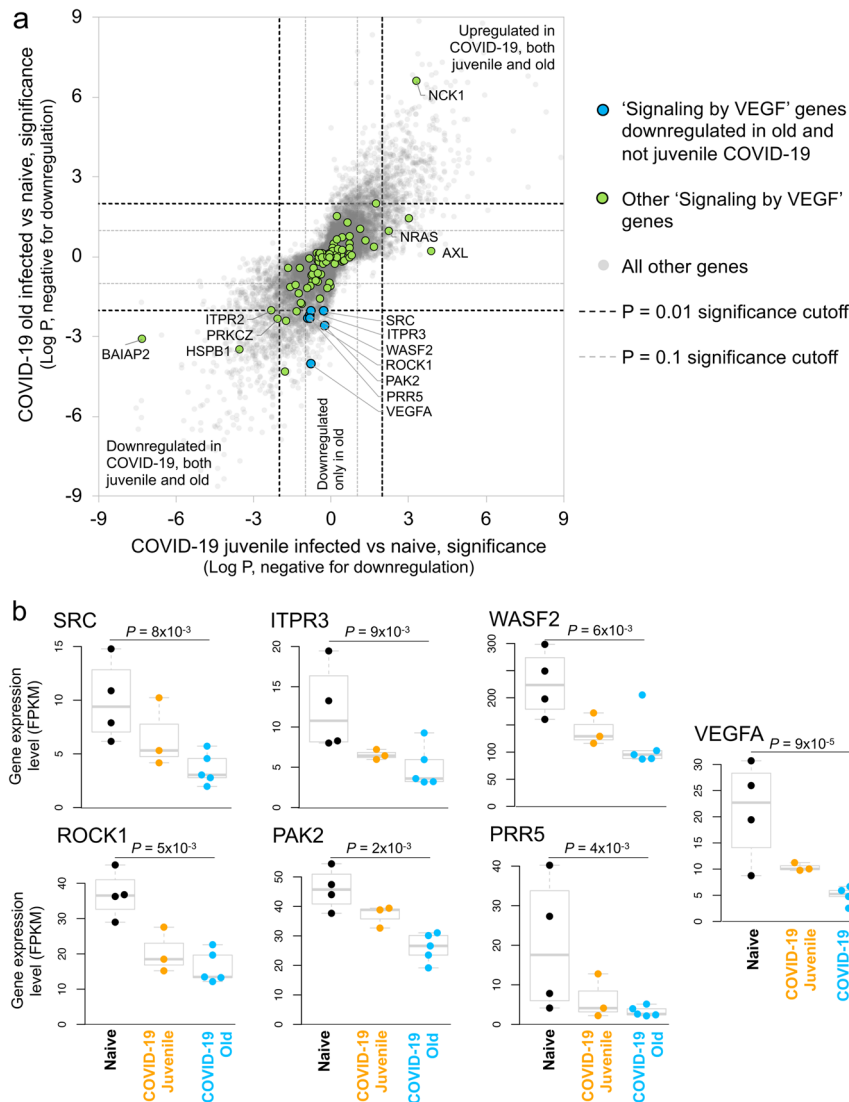


Fig. 7 VEGF pathway genes are significantly downregulated in old SARS-CoV-2-infected macaques but not juvenile SARS-CoV-2-infected macaques. **a** Differential expression significance values for genes from the “Signaling by VEGF” (R-HSA-194138) pathway, in both the juvenile vs naive and old vs naive comparisons. Included are significance values for all genes (gray), pathway genes significantly downregulated in old but not juvenile (orange) and other pathway genes (green). P value cutoffs (0.01 and 0.1) are indicated with dashed lines. **b** The relative expression levels (FPKM) for the seven “Signaling by VEGF” genes belonging to this gene set are shown. P values represent FDR-corrected significance values from DESeq2.

in PBMCs of humans infected with SARS-CoV-2 we found increased levels of VEGF and peripheral neutrophil counts in individuals >60 years when compared to younger individuals. These results together provide novel insights into the immunopathogenesis of COVID-19 disease, especially from the unique perspective of age as a contributing factor.

As we learn more about the pathophysiology of COVID-19, it is becoming clear that disease severity is associated with hyperinflammation which in turn induces lung and multiorgan injury and mortality via a cytokine storm^{1,2,51}. While therapeutic options that focus on immunomodulatory agents such as corticosteroids are being considered and used, immunomodulators may also inhibit protective pathways. Therefore, a thorough understanding of the host inflammatory responses during SARS-CoV-2 infection is needed before precise immunomodulators can be specifically designed to limit inflammation without regulating protective mechanisms of action. The distinct role of myeloid cells in COVID-19 lung injury and immunopathogenesis is beginning to be described in humans, where recruited

macrophages, inflammatory monocytes and neutrophils are associated with more severe COVID-19 disease and hyper-inflammatory cytokine environment^{8,9,11}. Furthermore, patients with COVID-19 exhibited hyper-inflammatory signatures across all types of cells among PBMCs, particularly upregulation of the TNF/IL-1 β -driven inflammatory response and type I IFN responses¹⁰. Indeed, we have clearly shown that neutrophils are recruited to the macaque lung after SARS-CoV-2 infection. Neutrophils play a protective role contributing to early antiviral defense⁵², but also can be pathological due to processes associated with degranulation and lysis, thereby promoting lung inflammation. Consistent with this notion, an increased peripheral neutrophil-to-lymphocyte ratio is observed in severe COVID-19 cases, and in some studies is also associated with unfavorable prognosis⁵³. These results in human studies are consistent with our macaque studies that describe neutrophil degranulation as one of the transcriptional pathways upregulated in the lungs of COVID-19 macaques when compared to uninfected controls. In this regard, the expression of *Cathepsin G* is noteworthy since it is

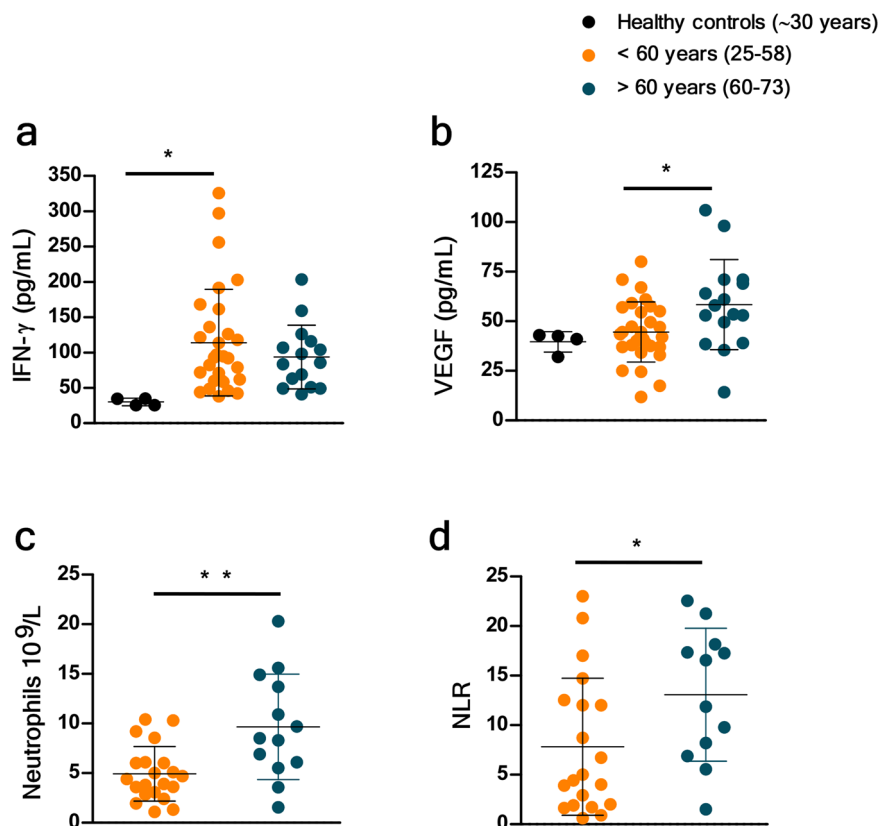


Fig. 8 VEGF and peripheral neutrophil counts are higher in old COVID-19 patients. Peripheral blood samples were obtained from a cohort of patients with laboratory-confirmed SARS-CoV-2 infection at hospital admission. Levels of different immune markers were determined by Luminex assay in plasma samples from COVID-19 and healthy volunteer controls. COVID-19 patients were stratified by age as younger than or older than 60 years. **a** Levels of IFN- γ and **b** levels of VEGF proteins were measured in plasma of COVID-19 and healthy controls. **c** Peripheral neutrophil counts and **d** neutrophil to lymphocyte ratio (NLR) values were retrieved from the medical records of COVID-19 patients and compared between age groups. Each point in the figure corresponds to an independent biological sample for each group. Mean \pm SD for each group is shown in the figure. Statistical significance was verified by one-way anova: $P = *(<0.05)$, $**(<0.01)$ with Tukey's correction (**a** and **b**) or by Student's *t*-test: $P = *(<0.05)$, $**(<0.01)$ (**c** and **d**).

a prominent serine protease that amplifies inflammation by stimulating the production of cytokines and chemokines that drive immune cell recruitment to the lung⁵⁴, and activates metalloproteases to cleave extracellular matrix proteins, thereby promoting neutrophil migration⁵⁵. Cathepsin G also induces potent chemotactic recruitment of monocytes, neutrophils and antigen-presenting cells in addition to promoting endothelial and epithelial permeability⁵⁶. The latter function of Cathepsin G could enhance viral invasion to extra-alveolar sites while increased epithelial permeability might also explain the gastrointestinal route of transmission¹⁶. In addition, ATP6AP2, causes the secretion of inflammatory and fibrotic factors³⁶, CD36, that induces neutrophil apoptosis, and CECAM8 whose cross-linking induces IL-8 production, all of which are highly expressed in COVID-19 diseased lungs. In patients with severe COVID-19, a higher frequency of CD66b⁺ neutrophils exist⁵⁷. Furthermore, our studies shed light on the importance of the membrane glycoprotein, CD36 in the response to SARS-CoV-2 infection. CD36 is expressed on platelets, macrophages, and even epithelial cells. In addition to its well-characterized apoptotic function, CD36 is also a receptor for thrombospondin-1 and related proteins and can function as a negative regulator of angiogenesis⁵⁸. This is particularly important given that angiogenesis is an important feature in patients with COVID-19 and associated ARDS⁵⁹. CD36 also binds long-chain fatty acids and facilitates their transport into cells, leading to muscle utilization, coupled with fat storage. This contributes to the pathogenesis of metabolic disorders, such

as diabetes and obesity and atherothrombotic disease⁵⁹. A recent single-cell analysis revealed significantly higher CD36 expression in association with ACE2-expressing human lung epithelial cells⁶⁰. Increased CD36 expression may therefore provide a protective role from an extreme lung injury during COVID-19, which is observed in the macaques. Our novel findings that CD36 (as well as other prominent signaling pathways) may be involved in the pathogenesis of COVID-19 has implications for host-directed therapy for SARS-CoV-2 infection. In contrast, neutrophils are recruited into the lung very early following macaque infection with SARS-CoV-2¹⁶. In addition, in the lungs of deceased individuals with severe COVID-19 disease, neutrophil infiltration occurred in pulmonary capillaries and was accompanied by extravasation of neutrophils into the alveolar space, and neutrophilic mucositis⁶¹. In the case of COVID-19, neutrophils could also be a source of excess neutrophil extracellular traps⁶². These results together suggest a scenario in the lung where induction of the cytokine storm drives the recruitment of neutrophils, thereby contributing to inflammation. Thus, degradation of neutrophils and formation of NETs may further promote cytokine responses and inflammation and disease immunopathogenesis.

The IFN response constitutes the major first line of defense against viruses. Recognition of viral infections by innate immune sensors activates both the type I and type III IFN response. While some studies have shown that serum of COVID-19 patients contains increased expression of proinflammatory cytokines and

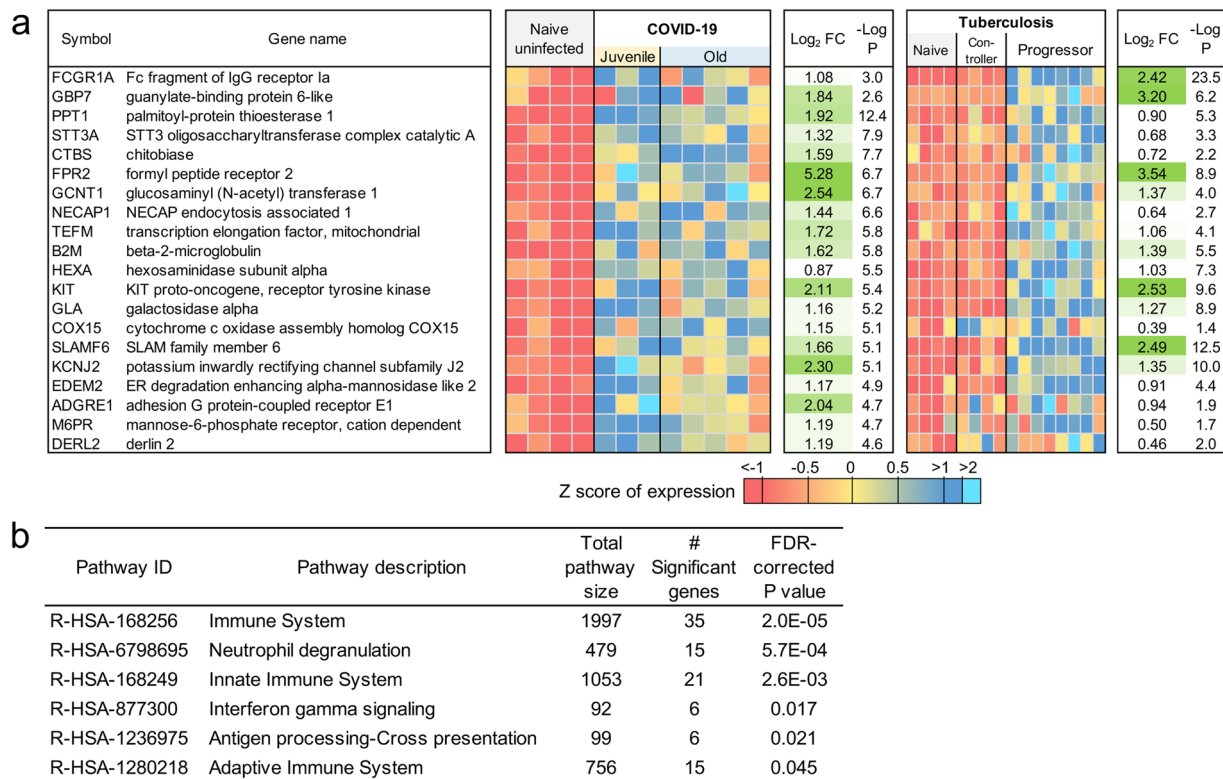


Fig. 9 Genes higher in expression during both COVID-19 and TB share common pathways. **a** The top 20 (of 97) most significantly upregulated genes in COVID-19 infected and TB infected macaques. Expression values are visualized by Z scores of normalized expression data (FPKM) per sample, and Log₂ fold change and -Log P values are from the DESeq2 output. Genes are sorted by P value. **b** Significant Reactome pathway enrichment among the 97 genes.

chemokines, without detectable levels of type I and III IFNs⁶³, other studies suggest that the IFN response may be delayed. Importantly, elevated IFNs correlate with more severe disease^{64,65}. Thus, it is unclear if type I IFNs are protective or pathological in COVID-19⁶⁶. It is possible that severe infection drives the higher expression of IFN pathway genes, but may not lead to viral containment, but instead drives pathological damage. On the other hand, increased induction of type I IFN pathways in SARS-CoV-2 infected macaques, as well as in juvenile macaques, could support a role for IFN signaling in protection rather than disease progression. Our studies provide data to support the recently proposed hypothesis that IFN induction may be compromised in older hosts⁶⁶. When the early IFN response is not optimal to control viral infection, it is possible that delayed or inadequate IFN responses may lead to inflammation-mediated damage. Further testing the protective versus pathological roles of IFNs in the macaque model with the availability of IFNAR blocking reagents should further clarify the specific role of IFN pathways in COVID-19.

ARDS in influenza, MERS, and SARS have been associated with fibrotic irreversible interstitial lung disease^{67,68}. Pulmonary fibrosis is a recognized sequelae of ARDS⁴². Pulmonary fibrosis can develop either following chronic inflammation or as a consequence of genetically associated and age-related fibroproliferative process, as in idiopathic pulmonary fibrosis (IPF)⁶⁹. Fibrosis is the hardening, and/or scarring of tissues due to excess deposition of extracellular matrix components including collagen. Since a significant proportion of COVID-19 patients develop severe ARDS, it is predicted that a similar outcome of fibrosis will be associated with COVID-19. Also, since the risk factors associated with COVID-19 including increasing age, male and associated co-morbidities coincide with risk factors, it is expected that COVID-19 patients will experience fibrotic lung disease. Despite

these associations, there is no evidence currently that “scarring of the lung” experienced by COVID-19 patients is fibrotic or progressive and an outcome of COVID-19 disease post recovery. Therefore, our results provide unique insights into the role of fibrosis during SARS-CoV-2 infection. Most notably, we find downregulation of collagen degradation pathways, as well as pathways associated with collagen formation, collagen trimerization, and assembly. Furthermore, the role of TGF-β and ECM degradation is well documented in fibrosis. Indeed, the genes associated with these pathways are also significantly downregulated. These results for the first time provide important insights into the early pathological events occurring during COVID-19 in the lungs with relevance to underlying immune mechanisms associated with canonical fibrosis pathways. While long-term consequences of the pulmonary COVID-19 such as fibrosis remain to be determined, our results on downregulation of collagen degradation and TGF-β pathways may represent important early events on the lungs of SARS-CoV-2 infected individuals.

Finally, we provide novel insights into the transcriptional regulation of immune pathways that are induced and regulated by age, an important risk factor for COVID-19 disease and outcome. This is a significant component of risk for disease and prognosis of COVID-19. We find higher induction of genes associated with Type I IFN signaling and Notch signaling in the young macaques. While we had sufficient macaque samples to compare young and old macaques, we do not have sufficient representation of both sexes to study sex-associated modulation of disease transcriptional profiles. Upregulation of these significant Type I IFN signaling genes suggest that in a model of self-limited clinical disease in macaques, Type I IFN induction may be differentially regulated by age-associated factors. Age-specific regulation of this pathway has been demonstrated in the murine model of TB⁷⁰. There is

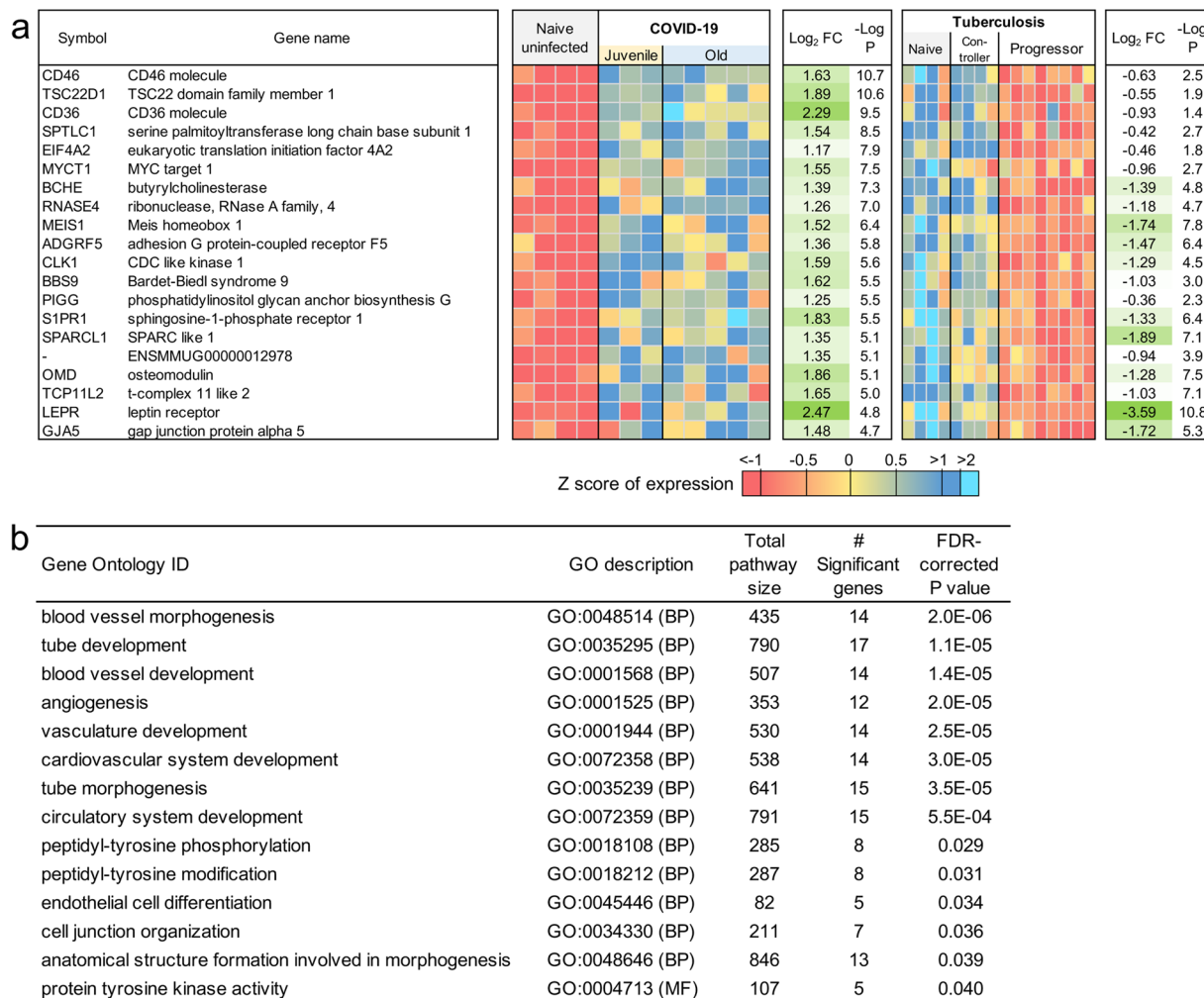


Fig. 10 Genes higher in expression during COVID-19 than TB are related to blood morphogenesis pathways. **a** The top 20 (of 76) most significantly upregulated genes in SARS-CoV-2-infected compared to *Mtb*-infected macaques. Expression values are visualized by Z scores of normalized expression data (FPKM) per sample, and Log₂ fold change and -Log P values are from the DESeq2 output. Genes are sorted by P value. **b** Significant Gene Ontology pathway enrichment among the 76 genes.

also a well-documented relationship between Notch signaling and viral infections. For example, Human Papilloma Virus and Simian Virus 40 can hijack the cellular machinery, including components of Notch signaling, and these events re-associated with cancer progression⁷¹. While innate and T cell responses are comparable between juvenile and old macaques following infection, SARS-CoV-2 specific antibody is generated at significantly higher levels in the plasma of juveniles, relative to old macaques¹⁶. Since Notch signaling regulates multiple stages of B-cell differentiation and shapes the antibody repertoire⁷², higher expression of many of the Notch pathway member genes in juvenile macaques may be responsible for the development of stronger antibody responses in these animals, impacting disease progression. Similarly, Type I IFN responses are critical for the downstream breadth of antibody production and recognition⁷³⁻⁷⁵. Thus, while T cell responses are comparable in juvenile and old macaques, differences in critical signaling pathways uncovered by our RNA-seq analysis potentially explain why juvenile macaques mount significantly stronger antibody responses, and consequently why younger subjects have reduced susceptibility to COVID-19. While this has not been recapitulated in the macaque model, older patients of COVID-19 are more susceptible to progression. This is consistent with increased disease progression when COVID-19 patients were stratified based

on age. A previous study found that peripheral VEGF concentrations were significantly higher in COVID-19 patients than in healthy controls⁷⁶. We also find this effect in our human samples (Fig. 8b) where people with COVID-19 that are older than 60 years of age have more VEGF protein in their peripheral blood. However, we also find significantly lower levels of VEGF pathway gene transcripts in the lungs of macaques with SARS-CoV-2 infection, especially older macaques (Fig. 6b and Fig. 7b). Our study further demonstrates that the changes in VEGF signaling may be associated with increasing age rather than just with disease severity. VEGF pathways promote angiogenesis and induce vascular leakiness and permeability. Our results therefore suggest that higher levels of VEGF in the periphery, while a biomarker for COVID-19, may be driven as a compensatory mechanism due to lower levels of VEGF signaling at the site of infection, i.e., the lung. These results further underscore the value of studying responses to SARS-CoV-2 infection in the lung compartment. By uncovering new aspects of the role of these signaling pathway in SARS-CoV-2 infection in the lung compared to the periphery using animal models and human samples, will shed further light on pathways that can be harnessed for therapeutics for COVID-19 disease.

TB and COVID-19 both primarily affect lung function. TB was already one of the leading causes of death due to an infectious

disease prior to the emergence of COVID-19. In the current scenario the clinical management of both TB and COVID together, particularly in the endemic regions is another rapidly emerging healthcare challenge needing immediate attention. Our results are the first to clearly demarcate the main differences in the manifestation of both the diseases in the alveolar niche. Neutrophil degranulation was one of the most significantly enriched pathways in both the disease conditions and therefore appears as a promising druggable target for efficient management of severe co-morbid TB COVID-19 condition. However, the selective enrichment of angiogenesis and vascular permeability in observed in the lungs of SARS-CoV-2 infected macaques is not seen in animal models, or patients of TB. These results have the potential to generate additional, specific druggable targets for COVID-19.

Overall, we interrogated transcriptional profiles of lungs from juvenile and old macaques infected with SARS-CoV-2. This study has provided fundamentally new information on the host response in young and old macaques infected with SARS-CoV-2. This model provides relevant insights necessary for further vaccine and therapeutic development for COVID-19.

Methods

Macaques. All of the infected animals were housed in Animal Biosafety Level 3 (ABSL3) at the Southwest National Primate Research Center, Texas Biomedical Research Institute, where they were treated per the standards recommended by AAALAC International and the NIH Guide for the Care and Use of Laboratory Animals. Sham controls were housed in ABSL2. The animal studies in each of the species were approved by the Animal Care and Use Committee of the Texas Biomedical Research Institute and as an omnibus Biosafety Committee protocol.

Animal studies, and tissue harvest for RNA sample preparation. Rhesus macaques (*Macaca mulatta*) animals enrolled in this study have been described in detail¹⁶, and the infection of these animals with 1.05×10^6 pfu SARS-CoV-2 isolate USA-WA1/2020 (BEI Resources, NR-52281, Manassas, VA) has also been described earlier¹⁶. Control (SARS-CoV-2 uninfected) samples were obtained from opportunistic necropsies conducted on rhesus macaques from the same colony in the past few months. Infected animals were euthanized for tissue collection at necropsy, including lung specimens. Lung tissue from three juvenile (3-yr old) and five old (average 17-yr old) rhesus macaques (Supplementary Data 1) were homogenized, snap-frozen in RLT buffer, and DNase-treated total RNA was extracted using the Qiagen RNeasy Mini kit (Qiagen) for RNA-seq analysis as described earlier⁵⁰.

Viral RNA determination. SARS-CoV-2 RNA isolation and measurement of viral RNA in lung homogenates using RTqPCR have been described¹⁶.

RNA-sequencing and analysis. cDNA libraries were prepared from RNA samples using the Clontech SMARTer universal low input RNA kit to maximize yield, and samples were sequenced on Illumina NovaSeq S4 XP (paired 150 bp reads). After adapter trimming using Trimmomatic v0.39⁷⁷, sequenced RNA-seq reads were aligned to the *Macaca mulatta* genome (version 10, Ensembl release 100⁷⁸) using the STAR aligner v2.7.3a⁷⁹ (2-pass mode, basic). All raw RNA-Seq fastq files were uploaded to the NCBI Sequence Read Archive (SRA⁸⁰), and complete sample metadata and accession information are provided in Supplementary Data 1. Read fragments (read pairs or single reads) were quantified per gene per sample using featureCounts v1.5.1⁸¹. Significantly differentially expressed genes between naive, controller, and progressor sample sets were identified using DESeq2 v1.4.5¹⁷ with default settings, and a minimum *P* value significance threshold of 0.01 (after False Discovery Rate [FDR⁸²] correction for the number of tests). PCA also was calculated using DESeq2 output (default settings, using the top 500 most variable genes). FPKM (fragments per kilobase of gene length per million reads mapped) normalization was performed using DESeq2-normalized read counts. Pathway enrichment analysis among differentially expressed gene sets of interest was performed for (a) Reactome¹⁸ pathways, using the human orthologs as input into the WebGestalt⁸³ web server ($p \leq 0.05$ after FDR correction, minimum 3 genes per term) and (b) KEGG¹⁹ pathways and Gene Ontology²⁰ terms, using the g:profiler web server⁸⁴ which has a database of these annotations matched to macaque ENSEMBL gene IDs ($p \leq 0.05$ after FDR correction, minimum 3 genes per term). Mapped fragment counts, relative gene expression levels, gene annotations, and differential expression data for every macaque gene are available in Supplementary Data 2, along with orthology matches to human genes retrieved from ENSEMBL⁷⁸ and identifications of differentially expressed (DE) genes belonging to enriched pathways of interest, for genes of interest in Supplementary Data 3, and significant

functional enrichment for Reactome, KEGG and Gene Ontology pathways, among differentially gene sets of interest in Supplementary Data 4. In addition, genes significantly differentially regulated during the progression of tuberculosis (in both the macaque gene and the corresponding mouse ortholog) were identified from a previous transcriptomic study of tuberculosis-infected lung tissue⁵⁰, and the upregulated and downregulated gene sets were intersected with the COVID-19 results from the current study.

Immunohistochemistry. Formalin-fixed paraffin-embedded non-human primate lung tissues were sectioned into 5- μ m thick cuts. Baking of sections was done at 65 °C with subsequent de-paraffinization using Xylene and re-hydration with decreasing gradations of ethanol and dH₂O. Heat-induced epitope retrieval method was used for antigen unmasking using Sodium citrate buffer (10 mM, pH 6.0) for 20 min at 95 °C. Sections were then blocked using 3% BSA in TBST at RT for 45 min. SARS CoV-2 Spike rabbit polyclonal antibody (ProSci, USA, 1:200, 2 h at 37 °C) and Mouse anti-human CD66abce-APC conjugated (Miltenyi Biotech, USA, 1:20, 2 h at 37 °C) were used for the detection of SARS CoV-2 virus and neutrophils, respectively. Goat anti-rabbit IgG (H + L), Alexa Fluor 488 conjugate secondary antibody (Thermo Fisher Scientific, USA, 1:400, 1 h at 37 °C) was used for labeling SARS CoV-2 Spike primary antibody. Further, specimens were incubated with DAPI for nuclear staining (Thermo Fisher Scientific, USA, 1:5000, 5 min at 37 °C) followed by mounting with Prolong Diamond Antifade mountant (Thermo Fisher Scientific, USA). The stained sections were then visualized using Zeiss LSM 800 confocal microscope ($\times 63$ magnification).

Human sample collection. Plasma samples were collected from COVID-19 patients that attended the emergency room of the Instituto Nacional de Ciencias Médicas y Nutrición Salvador Zubirán (INCMNSZ), and the Instituto Nacional de Enfermedades Respiratorias Ismael Cosío Villegas (INER) in Mexico City, from March to June of 2020. Detection of SARS-CoV-2 was performed by real-time polymerase chain reaction (RT-PCR) in swab samples, bronchial aspirates (BA), or bronchoalveolar lavage (BAL). For this purpose, viral RNA was extracted from clinical samples with the MagNA Pure 96 system (Roche, Penzberg, Germany). The RT-PCR reactions were performed in a total volume of 25 μ L, containing 5 μ L of RNA, 12.5 μ L of 2 \times reaction buffer provided with the Superscript III one-step RT-PCR system with Platinum Taq Polymerase (Invitrogen, Darmstadt, Germany; containing 0.4 mM of each deoxyribose triphosphates (dNTP) and 3.2 mM magnesium sulfate), 1 μ L of reverse transcriptase/ Taq mixture from the kit, 0.4 μ L of a 50 mM magnesium sulfate solution (Invitrogen), and 1 μ g of nonacetylated bovine serum albumin (Roche). All oligonucleotides were synthesized and provided by Tib-Molbiol (Berlin, Germany). Thermal cycling was performed at 55 °C for 10 min for reverse transcription, followed by 95 °C for 3 min and then 45 cycles of 95 °C for 15 s, 58 °C for 30 s. Primer and probe sequences are as follows: RdRp gene [RdRp-SARSr-F:GTGARATGGTCATGTGTGGCGG,RdRp-SARSr-P2: FAM-CAGGTGGAACCTCATCAGGAGATGCBQB,RdRp_SARSrP1:FAM-CAGGTGGWACRTCATCMGGTGATGCBQB,RdRp_SARSr:CAR-ATGTTAAASACACTATTAGCATA], E gene [E_Sarbeco_F: ACAGGTACGTTAATAGTTAATAGCGT,E_Sarbeco_P1:FAMA-CACTAGCCATCCTTACTGCGCTTCGBBQ,E_Sarbeco_R:ATATTGCAGCAG-TACGCACACA], N gene [N_Sarbeco_F:CACATTGGCACCCGCAATC, N_Sarbeco_P1:FAMACTTCTCAAGGAACAACATTGCCABBQ, N_Sarbeco_R: GAGGAACGAGAAGAGGCTTG]. Clinical and demographic data were retrieved from the medical records of all participants. These data included age, gender, anthropometrics, comorbidities, symptoms, triage vital signs, and initial laboratory test results. Initial laboratory tests were defined as the first test results available (typically within 24 h of admission) and included white blood cell counts (WBC), neutrophil, and lymphocyte counts (Supplementary Data 5). For human studies, written informed consent from participants under protocols approved by the Ethics Committee of the Instituto Nacional de Enfermedades Respiratorias Ismael Cosío Villegas, Mexico. The study was approved by the Institutional Research Committee of Instituto Nacional de Enfermedades Respiratorias Ismael Cosío Villegas, Mexico.

Cytokine levels in human plasma samples. Peripheral blood samples were obtained from all participants at hospital admission. Plasma levels of interferon-gamma (IFN- γ) and VEGF, were determined by Luminex assays using the Luminex platform Bio-Plex Multiplex 200 (Bio-Rad Laboratories, Inc., Hercules, CA, USA). Plasma samples from four healthy volunteer donors were used as controls.

Statistics and reproducibility. Where applicable, comparisons between two groups were performed using the unpaired two-tailed Student *t*-test, using the GraphPad Prism 5 software. In all instances, *P* values ≤ 0.05 were considered as significant. DESeq2 (version 1.4.5)¹⁷ with default settings, and a minimum *P* value significance threshold of 0.01 (after False Discovery Rate [FDR⁸²] correction for the number of tests was used for all RNA-Seq comparisons of differential expression.

Reporting summary. Further information on research design is available in the Nature Research Reporting Summary linked to this article.

Data availability

All processed data associated with this study are provided in the Supplementary Materials, and all unprocessed RNA-Seq reads are available for download from the NCBI Sequence Read Archive (SRA), BioProject PRJNA648493. Accession numbers and metadata per sample are provided in Supplementary Data 1, and processed read counts and normalized gene expression levels are provided in Supplementary Data 2.

Received: 3 September 2020; Accepted: 20 January 2021;

Published online: 05 March 2021

References

- Huang, C. et al. Clinical features of patients infected with 2019 novel coronavirus in Wuhan, China. *Lancet* **395**, 497–506 (2020).
- Xu, Z. et al. Pathological findings of COVID-19 associated with acute respiratory distress syndrome. *Lancet Respiratory Med.* **8**, 420–422 (2020).
- Tay, M. Z., Poh, C. M., Renia, L., MacAry, P. A. & Ng, L. F. P. The trinity of COVID-19: immunity, inflammation and intervention. *Nat. Rev. Immunol.* <https://doi.org/10.1038/s41577-020-0311-8> (2020).
- Vabret, N. et al. The Sinai Immunology Review Project. Immunology of COVID-19: current state of the science. *Immunity* <https://doi.org/10.1016/j.immuni.2020.05.002> (2020).
- Monaco, G. et al. RNA-Seq signatures normalized by mrna abundance allow absolute deconvolution of human immune cell types. *Cell Rep.* **26**, 1627–1640. e1627 (2019).
- Wilson, J. A. et al. RNA-Seq analysis of chikungunya virus infection and identification of granzyme A as a major promoter of arthritic inflammation. *PLoS Pathog.* **13**, e1006155 (2017).
- Xiong, Y. et al. Transcriptomic characteristics of bronchoalveolar lavage fluid and peripheral blood mononuclear cells in COVID-19 patients. *Emerg. Microbes Infect.* **9**, 761–770 (2020).
- Bost, P. et al. Host-viral infection maps reveal signatures of severe COVID-19 patients. *Cell* **181**, 1475–1488. e1412 (2020).
- Chua, R. L. et al. COVID-19 severity correlates with airway epithelium-immune cell interactions identified by single-cell analysis. *Nat. Biotechnol.* **38**, 970–979 (2020).
- Lee, J. S. et al. Immunophenotyping of COVID-19 and influenza highlights the role of type I interferons in development of severe COVID-19. *Sci. Immunol.* **5**, eabd1554 (2020).
- Schulte-Schrepping, J. et al. Severe COVID-19 is marked by a dysregulated myeloid cell compartment. *Cell* **182**, 1419–1440. e1423 (2020).
- Ziegler, C. G. K. et al. SARS-CoV-2 receptor ACE2 Is an interferon-stimulated gene in human airway epithelial cells and is detected in specific cell subsets across tissues. *Cell* **181**, 1016–1035. e1019 (2020).
- Liao, M. et al. Single-cell landscape of bronchoalveolar immune cells in patients with COVID-19. *Nat. Med.* **26**, 842–844 (2020).
- Wilk, A. J. et al. A single-cell atlas of the peripheral immune response in patients with severe COVID-19. *Nat. Med.* <https://doi.org/10.1038/s41591-020-0944-y> (2020).
- Zheng, Z. et al. Risk factors of critical & mortal COVID-19 cases: a systematic literature review and meta-analysis. *J. Infection* <https://doi.org/10.1016/j.jinf.2020.04.021> (2020).
- Singh, D. K. et al. Responses to acute infection with SARS-CoV-2 in the lungs of rhesus macaques, baboons and marmosets. *Nat. Microbiol.* <https://doi.org/10.1038/s41564-020-00841-4> (2020).
- Anders, S. & Huber, W. Differential expression analysis for sequence count data. *Genome Biol.* **11**, R106 (2010).
- Fabregat, A. et al. The reactome pathway knowledgebase. *Nucleic Acids Res.* **46**, D649–D655 (2018).
- Kanehisa, M., Sato, Y., Furumichi, M., Morishima, K. & Tanabe, M. New approach for understanding genome variations in KEGG. *Nucleic Acids Res.* **47**, D590–D595 (2019).
- The Gene Ontology, C. The Gene Ontology Resource: 20 years and still GOing strong. *Nucleic Acids Res.* **47**, D330–D338 (2019).
- Sakatsume, M. et al. The Jak kinases differentially associate with the alpha and beta (accessory factor) chains of the interferon gamma receptor to form a functional receptor unit capable of activating STAT transcription factors. *J. Biol. Chem.* **270**, 17528–17534 (1995).
- Aguet, M., Dembić, Z. & Merlin, G. Molecular cloning and expression of the human interferon-gamma receptor. *Cell* **55**, 273–280 (1988).
- Walter, M. R. et al. Crystal structure of a complex between interferon-gamma and its soluble high-affinity receptor. *Nature* **376**, 230–235 (1995).
- Thiel, D. J. et al. Observation of an unexpected third receptor molecule in the crystal structure of human interferon-gamma receptor complex. *Structure* **8**, 927–936 (2000).
- Olejnik, J., Hume, A. J. & Muhlberger, E. Toll-like receptor 4 in acute viral infection: too much of a good thing. *PLoS Pathog.* **14**, e1007390 (2018).
- Wang, J. & Li, Y. CD36 tango in cancer: signaling pathways and functions. *Theranostics* **9**, 4893–4908 (2019).
- Ocklind, G., Friedrichs, D. & Peters, J. H. Expression of CD54, CD58, CD14, and HLA-DR on macrophages and macrophage-derived accessory cells and their accessory capacity. *Immunol. Lett.* **31**, 253–258 (1992).
- Moingeon, P. et al. CD2-mediated adhesion facilitates T lymphocyte antigen recognition function. *Nature* **339**, 312–314 (1989).
- Dengler, T. J. et al. Structural and functional epitopes of the human adhesion receptor CD58 (LFA-3). *Eur. J. Immunol.* **22**, 2809–2817 (1992).
- Dustin, M. L., Selvaraj, P., Mattaliano, R. J. & Springer, T. A. Anchoring mechanisms for LFA-3 cell adhesion glycoprotein at membrane surface. *Nature* **329**, 846–848 (1987).
- Gollob, J. A. et al. Molecular interaction between CD58 and CD2 counter-receptors mediates the ability of monocytes to augment T cell activation by IL-12. *J. Immunol.* **157**, 1886–1893 (1996).
- Selvaraj, P. et al. The T lymphocyte glycoprotein CD2 binds the cell surface ligand LFA-3. *Nature* **326**, 400–403 (1987).
- Springer, T. A., Dustin, M. L., Kishimoto, T. K. & Marlin, S. D. The lymphocyte function-associated LFA-1, CD2, and LFA-3 molecules: cell adhesion receptors of the immune system. *Annu. Rev. Immunol.* **5**, 223–252 (1987).
- Rolle, A. et al. CD2-CD58 interactions are pivotal for the activation and function of adaptive natural killer cells in human cytomegalovirus infection. *Eur. J. Immunol.* **46**, 2420–2425 (2016).
- Leitner, J., Herndler-Brandstetter, D., Zlabinger, G. J., Grubeck-Loebenstien, B. & Steinberger, P. CD58/CD2 is the primary costimulatory pathway in human CD28-CD8+ T cells. *J. Immunol.* **195**, 477–487 (2015).
- Rafiq, K., Mori, H., Masaki, T. & Nishiyama, A. (Pro)renin receptor and insulin resistance: possible roles of angiotensin II-dependent and -independent pathways. *Mol. Cell. Endocrinol.* **378**, 41–45 (2013).
- Schroder, A. K., Uciechowski, P., Fleischer, D. & Rink, L. Crosslinking of CD66B on peripheral blood neutrophils mediates the release of interleukin-8 from intracellular storage. *Hum. Immunol.* **67**, 676–682 (2006).
- Tcherniuk, S. et al. Formyl peptide receptor 2 plays a deleterious role during influenza A virus infections. *J. Infect. Dis.* **214**, 237–247 (2016).
- Amat, M. et al. Evolution of leukotriene B4, peptide leukotrienes, and interleukin-8 plasma concentrations in patients at risk of acute respiratory distress syndrome and with acute respiratory distress syndrome: mortality prognostic study. *Crit. Care Med.* **28**, 57–62 (2000).
- Saftig, P., Beertsen, W. & Eskelinen, E. L. LAMP-2: a control step for phagosome and autophagosome maturation. *Autophagy* **4**, 510–512 (2008).
- Wu, C. et al. Risk factors associated with acute respiratory distress syndrome and death in patients with coronavirus disease 2019 pneumonia in Wuhan, China. *JAMA Internal Med.* <https://doi.org/10.1001/jamainternmed.2020.0994> (2020).
- Spagnolo, P. et al. Pulmonary fibrosis secondary to COVID-19: a call to arms? *Lancet Respir. Med.* [https://doi.org/10.1016/S2213-2600\(20\)30222-8](https://doi.org/10.1016/S2213-2600(20)30222-8) (2020).
- Meduri, G. U. et al. Persistent elevation of inflammatory cytokines predicts a poor outcome in ARDS. Plasma IL-1 beta and IL-6 levels are consistent and efficient predictors of outcome over time. *Chest* **107**, 1062–1073 (1995).
- Bartram, U. & Speer, C. P. The role of transforming growth factor beta in lung development and disease. *Chest* **125**, 754–765 (2004).
- Lambert, D. W. et al. Tumor necrosis factor-alpha convertase (ADAM17) mediates regulated ectodomain shedding of the severe-acute respiratory syndrome-coronavirus (SARS-CoV) receptor, angiotensin-converting enzyme-2 (ACE2). *J. Biol. Chem.* **280**, 30113–30119 (2005).
- Steinbuck, M. P. & Winandy, S. A review of notch processing with new insights into ligand-independent notch signaling in T-cells. *Front. Immunol.* **9**, 1230 (2018).
- Merad, M. & Martin, J. C. Pathological inflammation in patients with COVID-19: a key role for monocytes and macrophages. *Nat. Rev. Immunol.* **20**, 355–362 (2020).
- Zhang, Q. et al. ACE2 inhibits breast cancer angiogenesis via suppressing the VEGFa/VEGFR2/ERK pathway. *J. Exp. Clin. Cancer Res.* **38**, 173 (2019).
- Yu, X. et al. ACE2 antagonizes VEGFa to reduce vascular permeability during acute lung injury. *Cell. Physiol. Biochem.* **38**, 1055–1062 (2016).
- Ahmed, M. et al. Immune correlates of tuberculosis disease and risk translate across species. *Sci. Transl. Med.* <https://doi.org/10.1126/scitranslmed.aay0233> (2020).
- Didangelos, A. COVID-19 hyperinflammation: what about neutrophils? *mSphere* <https://doi.org/10.1128/mSphere.00367-20> (2020).
- Camp, J. V. & Jonsson, C. B. A role for neutrophils in viral respiratory disease. *Front. Immunol.* **8**, 550 (2017).

53. Zheng, M. et al. Functional exhaustion of antiviral lymphocytes in COVID-19 patients. *Cell. Mol. Immunol.* **17**, 533–535 (2020).
54. Steinwede, K. et al. Cathepsin G and neutrophil elastase contribute to lung-protective immunity against mycobacterial infections in mice. *J. Immunol.* **188**, 4476–4487 (2012).
55. Son, E. D. et al. Cathepsin G increases MMP expression in normal human fibroblasts through fibronectin fragmentation, and induces the conversion of proMMP-1 to active MMP-1. *J. Dermatol. Sci.* **53**, 150–152 (2009).
56. Gao, S., Zhu, H., Zuo, X. & Luo, H. Cathepsin G and its role in inflammation and autoimmune diseases. *Arch. Rheumatol.* **33**, 498–504 (2018).
57. Morrissey, S. M. et al. Emergence of low-density inflammatory neutrophils correlates with hypercoagulable state and disease severity in COVID-19 patients. Preprint at *medRxiv* <https://doi.org/10.1101/2020.05.22.20106724> (2020).
58. Silverstein, R. L. & Febbraio, M. CD36, a scavenger receptor involved in immunity, metabolism, angiogenesis, and behavior. *Sci. Signal* **2**, re3 (2009).
59. Ackermann, M. et al. Pulmonary vascular endothelialitis, thrombosis, and angiogenesis in Covid-19. *N. Engl. J. Med.* **383**, 120–128 (2020).
60. Han, L. et al. Single-cell atlas of a non-human primate reveals new pathogenic mechanisms of COVID-19. *bioRxiv* <https://doi.org/10.1101/2020.04.10.022103> (2020).
61. Barnes, B. J. et al. Targeting potential drivers of COVID-19: Neutrophil extracellular traps. *J. Exp. Med.* <https://doi.org/10.1084/jem.20200652> (2020).
62. Kuznetsova, A., Brockhoff, P. B. & Christensen, R. H. B. lmerTest Package: tests in linear mixed effects models. *J. Stat. Softw.* **82**, 1–26 (2017).
63. Blanco-Melo, D. et al. Imbalanced host response to SARS-CoV-2 drives development of COVID-19. *Cell* **181**, 1036–1045.e1039 (2020).
64. Cameron, M. J. et al. Interferon-mediated immunopathological events are associated with atypical innate and adaptive immune responses in patients with severe acute respiratory syndrome. *J. Virol.* **81**, 8692–8706 (2007).
65. Zuo, W., Zhao, X. & Chen, Y. G. SARS coronavirus and lung fibrosis. *Mol. Biol. SARS-coronavirus* https://doi.org/10.1007/978-3-642-03683-5_15 (2009).
66. Park, A. & Iwasaki, A. Type I and type III interferons - induction, signaling, evasion, and application to combat COVID-19. *Cell Host Microbe* **27**, 870–878 (2020).
67. Blondonnet, R., Constantin, J. M., Sapin, V. & Jabaudon, M. A pathophysiologic approach to biomarkers in acute respiratory distress syndrome. *Dis. Markers* **2016**, 3501373 (2016).
68. Perlman, S. & Dandekar, A. A. Immunopathogenesis of coronavirus infections: implications for SARS. *Nat. Rev. Immunol.* **5**, 917–927 (2005).
69. George, P. M., Wells, A. U. & Jenkins, R. G. Pulmonary fibrosis and COVID-19: the potential role for antifibrotic therapy. *Lancet Respir. Med.* [https://doi.org/10.1016/S2213-2600\(20\)30225-3](https://doi.org/10.1016/S2213-2600(20)30225-3) (2020).
70. Tripathi, D. et al. Alcohol enhances type I interferon- α production and mortality in young mice infected with *Mycobacterium tuberculosis*. *PLOS Pathog.* **14**, e1007174 (2018).
71. Rizzo, P. et al. COVID-19 in the heart and the lungs: could we “Notch” the inflammatory storm? *Basic Res. Cardiol.* **115**, 31 (2020).
72. Cruickshank, M. N. & Ulgiate, D. The role of notch signaling in the development of a normal B-cell repertoire. *Immunol. Cell Biol.* **88**, 117–124 (2010).
73. Domeier, P. P. et al. B-cell-intrinsic type I interferon signaling is crucial for loss of tolerance and the development of autoreactive B cells. *Cell Rep.* **24**, 406–418 (2018).
74. Kiefer, K., Oropallo, M. A., Cancro, M. P. & Marshak-Rothstein, A. Role of type I interferons in the activation of autoreactive B cells. *Immunol. Cell Biol.* **90**, 498–504 (2012).
75. Vasconcellos, R., Braun, D., Coutinho, A. & Demengeot, J. Type I IFN sets the stringency of B cell repertoire selection in the bone marrow. *Int. Immunol.* **11**, 279–288 (1999).
76. Costela-Ruiz, V. J., Illescas-Montes, R., Puerta-Puerta, J. M., Ruiz, C. & Melguizo-Rodriguez, L. SARS-CoV-2 infection: the role of cytokines in COVID-19 disease. *Cytokine Growth Factor Rev.* <https://doi.org/10.1016/j.cytogfr.2020.06.001> (2020).
77. Bolger, A. M., Lohse, M. & Usadel, B. Trimmomatic: a flexible trimmer for Illumina sequence data. *Bioinformatics* **30**, 2114–2120 (2014).
78. Yates, A. D. et al. Ensembl 2020. *Nucleic Acids Res.* **48**, D682–D688 (2020).
79. Dobin, A. et al. STAR: ultrafast universal RNA-seq aligner. *Bioinformatics* **29**, 15–21 (2013).
80. Leinonen, R., Sugawara, H. & Shumway, M., on behalf of the International Nucleotide Sequence Database, C. The Sequence Read Archive. *Nucleic Acids Res.* **39**, D19–D21 (2011).
81. Liao, Y., Smyth, G. K. & Shi, W. featureCounts: an efficient general purpose program for assigning sequence reads to genomic features. *Bioinformatics* **30**, 923–930 (2014).
82. Benjamini, Y. & Hochberg, Y. Controlling the false discovery rate: a practical and powerful approach to multiple testing. *J. R. Stat. Soc. Ser. B Stat. Methodol.* **57**, 289–300 (1995).
83. Wang, J., Vasaikar, S., Shi, Z., Greer, M. & Zhang, B. WebGestalt 2017: a more comprehensive, powerful, flexible and interactive gene set enrichment analysis toolkit. *Nucleic Acids Res.* **45**, W130–W137 (2017).
84. Raudvere, U. et al. g:Profiler: a web server for functional enrichment analysis and conversions of gene lists (2019 update). *Nucleic Acids Res.* **47**, W191–W198 (2019).

Acknowledgements

NHP samples used in this work were derived from studies supported by intramural funds raised by Texas Biomedical Research Institute towards its Coronavirus Working Group, by Regeneron, Inc. (R.C., contract # 2020_004110, in part with federal funds from the Department of Health and Human Services; Office of the Assistant Secretary for Preparedness and Response; Biomedical Advanced Research and Development Authority, under Contract No. HHSO100201700020C). The work described in this manuscript was supported by Washington University in St. Louis (S.A.K.) for COVID-19 research, as well as and NIH award # R01AI123780 to S.A.K., M.M., and D.K., R01AI134236 to S.A. K. and D.K. and a COVID Grant Number: 3R01AI134236 - 04W1., and by institutional NIH awards P51OD111033 and U42OD010442 to the SNPRC, Texas Biomedical Research Institute. J.A.P.-C. was supported by the National Council of Science and Technology of Mexico to achieve (CONACYT) his PhD degree (CONACyT-CVU 737347). The current study was supported by institutional research funds of INER and by research contracts: SECTEI/050/2020, Secretaría de Ciencia, Tecnología e Innovación de la Ciudad de México (SECTEI CDMX); FORDECYT/10SE/2020/05/14-06 and FORDECYT/10SE/2020/05/14-07 from the Fondo Institucional de Fomento Regional para el Desarrollo Científico y Tecnológico y de Innovación (FORDECYT), Consejo Nacional de Ciencia y Tecnología (CONACYT). These funders had no role, however, in the design and execution of the experiments and the interpretation of data. The views expressed here are those of the authors and do not necessarily represent the views or official position of the funding agencies.

Author contributions

B.A.R., M.A., D.S., J.C., B.S., J.M., O. G, J.A.C.-P., L.A.J.-A., T.S.R.-R., and J.Z. carried out experiments, analyzed data; J.Z., L.S.S., R.C., M.M., D.K., and S.A.K designed the study, provided funding or reagents; M.A., B.A.R., D.K., and S.A.K wrote the paper; all authors read, edited and approved the manuscript.

Competing interests

The authors declare no competing interests.

Additional information

Supplementary information The online version contains supplementary material available at <https://doi.org/10.1038/s42003-021-01829-4>.

Correspondence and requests for materials should be addressed to M.M., D.K. or S.A.K.

Reprints and permission information is available at <http://www.nature.com/reprints>

Publisher's note Springer Nature remains neutral with regard to jurisdictional claims in published maps and institutional affiliations.



Open Access This article is licensed under a Creative Commons Attribution 4.0 International License, which permits use, sharing, adaptation, distribution and reproduction in any medium or format, as long as you give appropriate credit to the original author(s) and the source, provide a link to the Creative Commons license, and indicate if changes were made. The images or other third party material in this article are included in the article's Creative Commons license, unless indicated otherwise in a credit line to the material. If material is not included in the article's Creative Commons license and your intended use is not permitted by statutory regulation or exceeds the permitted use, you will need to obtain permission directly from the copyright holder. To view a copy of this license, visit <http://creativecommons.org/licenses/by/4.0/>.

© The Author(s) 2021